

DTIC FILE COPY

MIL-STD-847B

7 November 1983  
Unclassified

SECURITY CLASSIFICATION OF THIS PAGE

REPORT DOCUMENTATION PAGE				
1a. REPORT SECURITY CLASSIFICATION Unclassified			1b. RESTRICTIVE MARKINGS	
2a. SECURITY CLASSIFICATION AUTHORITY			3. DISTRIBUTION/AVAILABILITY OF REPORT Approved for public release Distribution is Unlimited	
2b. DECLASSIFICATION/DOWNGRADING SCHEDULE			5. MONITORING ORGANIZATION REPORT NUMBER(S) NA	
4. PERFORMING ORGANIZATION REPORT NUMBER(S) NA			7a. NAME OF MONITORING ORGANIZATION Center for Night Vision and Electro-Optics	
6a. NAME OF PERFORMING ORGANIZATION Univ. of N. Texas		6b. OFFICE SYMBOL (If applicable)	7b. ADDRESS (City, State and ZIP Code) ATTN: AMSEL-RD-NV-IRT Fort Belvoir, VA 22060-5677	
8a. NAME OF FUNDING/SPONSORING ORGANIZATION CNVEO			8b. OFFICE SYMBOL (If applicable) AMSEL-RD-NV-IT	9. PROCUREMENT INSTRUMENT IDENTIFICATION NUMBER DAAB07-87-C-F094
8c. ADDRESS (City, State and ZIP Code) Fort Belvoir, VA 22060-5677			10. SOURCE OF FUNDING NOS	
11. TITLE (Include Security Classification) <b>ABSORPTION</b> Two Photon Characterization			PROGRAM ELEMENT NO. 661102A	PROJECT NO. 1L16110 2A31B
12. PERSONAL AUTHOR(S) David G. Seiler			TASK NO. HO	WORK UNIT NO. 007-CJ
13a. TYPE OF REPORT Interim		13b. TIME COVERED FROM 11/87 TO 2/88	14. DATE OF REPORT (Yr, Mo, Day) 7/88	
15. PAGE COUNT 23				
16. SUPPLEMENTARY NOTATION				
17. COSATI CODES			18. SUBJECT TERMS (Continue on reverse if necessary and identify by block number)	
FIELD 7	GROUP 05	SUB. GR.	Defect characterization, Magneto-optical measurements, Two Photon Spectroscopy, Narrow band gap semiconductors, II-VI compounds,	
19. ABSTRACT (Continue on reverse if necessary and identify by block number) Magneto-Optical studies of HgCdTe have provided a rich new group of spectroscopies for studying defects and impurities in narrow band semiconductors such as HgCdTe.				
20. DISTRIBUTION/AVAILABILITY OF ABSTRACT UNCLASSIFIED/UNLIMITED <input checked="" type="checkbox"/> SAME AS RPT. <input type="checkbox"/> DTIC USERS <input type="checkbox"/>			21. ABSTRACT SECURITY CLASSIFICATION Unclassified	
22a. NAME OF RESPONSIBLE INDIVIDUAL Frederick F. Carlson			22b. TELEPHONE NUMBER (Include Area Code) 703-664-5036	22c. OFFICE SYMBOL AMSEL-RD-NV-IT

DTIC  
ELECTE  
AUG 24 1988  
S E D

DD FORM 1473, 83 APR

EDITION OF 1 JAN 73 IS OBSOLETE.

Unclassified

SECURITY CLASSIFICATION OF THIS PAGE

Figure 8. Report Documentation Page, DD Form 1473 (1 of 2)

①

511-5031

Performance Report

November 28, 1987 - February 27, 1988

Second Quarter (Three Months)

Contract DAAB07-87-C-FO94

With U. S. Army Night Vision and Electro-Optics Center

Fort Belvoir, Virginia 22060-5677

Contract Monitor: Dr. Fred Carlson

"Two-Photon Absorption Characterization"

Principal Investigator: Dr. David G. Seiler

Center for Applied Quantum Electronics

Department of Physics

University of North Texas

Denton, Texas 76203

The views, opinions, and/or findings contained in this report are those of the author and should not be construed as an official Department of the Army position, policy or decision, unless designated by other documentation.

Performance Report  
November 28, 1987 - February 27, 1988  
Second Quarter (Three Months)

Contract DAAB07-87-C-FO94

"Two-Photon Absorption Characterization"

P.I., Dr. David G. Seiler  
University of North Texas

Accession For	
NTIS	GRA&I <input checked="" type="checkbox"/>
DTIC TAB	<input type="checkbox"/>
Unannounced	<input type="checkbox"/>
Justification	
By	
Distribution/	
Availability Codes	
Dist	Avail and/or Special
A-1	

According to the Time Phase Task Schedule on p. 26 of the proposed Technical Work, our research investigation and sample characterization has proceeded along four task categories:

- (a) Build an experimental facility specifically designed for the characterization of HgCdTe with special emphasis given to infrared laser systems, variable low temperature and liquid helium techniques, and high magnetic fields.
- (b) Investigate two-photon absorption.
- (e) Investigate time resolved behavior in HgCdTe excited by two-photon absorption, and estimate the lifetimes of charge carriers.
- (f) Analyze the "lifetime" data to determine both surface and bulk recombination probabilities.

This report will address progress made to date in each of the tasks.

I. (a) Experimental Facility.

Facilities have been assembled that are capable of obtaining high magnetic fields (0-120 kG) and low temperatures with infrared and far infrared laser light. The experimental design and construction has been shown to be reliable and useful in the study of two-photon absorption processes in narrow band semiconductors, and specifically in HgCdTe (see Part II of this report). Naturally, improvements in the optical layout and components, and in the signal-to-noise ratio of the system, will be continually sought.

II. (b) Investigate Two-Photon Absorption.

A major breakthrough has been achieved this quarter - two-photon magneto-absorption spectra have been obtained for bulk samples of HgCdTe. To our knowledge, this is the first report of such spectra. Other magneto-optical structure has been observed that is due to: (1) impurities and/or defects; (2) one-photon interband magneto-absorption. In addition, unusual structure has been observed at high incident photon intensities. The data we have gathered can be summarized by sample:

n - HgCdTe,  $x = 0.236$  (at 77K,  $n = 1.4 \times 10^{14} \text{cm}^{-3}$  and  $\mu = 1.6 \times 10^5 \text{cm}^2/\text{Vsec}$

This bulk sample was obtained from Honeywell, and was the subject of our most intense investigations. Figure 1 shows the photoconductive response of the sample as a function of magnetic field for various incident laser photon energies. The data shows two large peaks representing two-photon absorption (TPA) processes between 80-120 kG. These absorption peaks are attributable to electron transitions between the valence band and conduction band Landau levels. Note how the positions of the peaks change with incident photon energy, since for differing values of photon energy, the magnetic field at which the TPA resonance occurs is different. These same two resonances have been observed in every sample of HgCdTe studied to date, thus their proper identification (in terms of exactly which final and initial Landau levels are responsible for each transition is vital.

At lower magnetic fields, other absorption processes occur, as shown in Figure 2. Multiple resonances in the photoconductive response are due to one-photon magneto-absorption (OPMA) processes. OPMA spectra can be used (in combination with TPA spectra) to accurately determine the band gap and  $x$  value of HgCdTe, and can be used to aid in the identification of other absorption processes, such as those arising from impurity levels. The broad structure shown in Figure 2 is identified as an acceptor-level-to-conduction-band (ACB) transition. Evidence in support of this identification comes from two facts: (1) the ACB structure is almost non-existent at low intensities - where the OPMA transition dominates; (2) As shown in Figure 3, the amplitude of the ACB structure is much more dependent on temperature than that of the OPMA transitions.

Finally, some extremely unusual structure was observed at high incident photon intensities, as shown in Figure 4. This structure appears just below (in magnetic field) the OPMA transition. At low intensities, the OPMA structure dominates, while at high intensities, the spectra is a superposition of the OPMA and ACB spectra with this unusual structure. The photon energy dependence of this structure is shown in Figure 5 with a scale expanded in magnetic field. Note that the resonance positions of this structure change little with photon energy. For now we note that this structure is real and will spend time on interpreting it later.

Figure 6 shows a plot of incident photon energy vs. the magnetic field position of all of the photoconductive resonances observed (except for the unusual, high intensity structure). Those points occurring at high magnetic fields are due to TPA, and thus should be plotted as  $2 \hbar\omega$ . In the future, a modified 8 x 8 Pidgeon and Brown model will be used to calculate the theoretical energies at which all of these transitions occur which will quantitatively explain this data.

n - HgCdTe  $x = 0.26$ .

This sample was obtained from Cominco. It had the following characteristics:

300K - IR - TCO (x min = 0.258)  
(x max = 0.261)

300K mobility =  $7.3 \times 10^3 \text{cm}^2/\text{Vsec}$   
concentration =  $7.2 \times 10^{15}$  electrons

77K mobility =  $7.6 \times 10^4$   
concentration =  $1.0 \times 10^{14}$

Crystal p4100.60

We have attached Cominco's transmission plots for this sample as Figure 7. Figure 8 shows the photoconductive response vs. magnetic field. Again, the two, high magnetic field resonances are clearly seen, which we identify as TPA transitions. At this writing, our investigations of this sample have been limited to confirming that the two-photon absorption processes seen in the Honeywell

sample can be seen in other samples.

$$\text{n - HgCdTe } x = 0.277.$$

This sample was also received from Cominco, and again their transmission data is enclosed (as Figure 9). Figure 10 shows the photoconductive response vs. magnetic field for this sample. Again, the two large TPA resonances can be seen. It had the following characteristics:

300K - IR - TCO  
(x min = 0.276)  
(x max = 0.278)

300K mobility =  $5.8 \times 10^3 \text{ cm}^2/\text{Vsec}$   
concentration =  $5.2 \times 10^{15}$  electrons

77K mobility =  $6.6 \times 10^4$   
concentration =  $1.4 \times 10^{14}$

Crystal 15(603)-51

### Summary of Progress

We have reported the first observation of two-photon magneto-absorption in samples of HgCdTe with differing  $x$  values, and have identified acceptor level to conduction band transitions. This information will allow us to identify and study other resonances, including those from impurity and/or defect levels.

### III. (e) Time Resolved Behavior... and (f) "Lifetime" data.

Work is proceeding in two main areas: (1) The development of a novel method to determine true minority carrier lifetimes in p-type narrow gap materials; and (2) the investigation of laser-induced impurity absorption processes in p-type material (with the goal of determining the individual absorption and recombination coefficients of impurity and defect levels along with the concentration of deep levels). Progress in these areas is summarized as follows:

#### (1) Novel methodology to determine minority carrier lifetimes.

We have recently developed a novel method to obtain information about multi-carrier semiconductor systems (see Appl. Phys. Lett., 51, 1916, 1987; a copy of which is attached). Using an analysis of the magnetoconductivity tensor components, the carrier concentration and mobility of both majority and minority carriers can be easily obtained.

Although the method was first applied to multi-carrier analysis in dark, thermal equilibrium conditions, it is also applicable to the analysis and study of photo-excited carriers under laser excitation conditions. This permits the extraction of "true" minority carrier lifetimes in p-type semiconductors (as opposed to the somewhat ambiguous results typically obtained from using photoconductivity techniques alone).

A relatively simple system - p-InSb - was first used to prove the effectiveness of the method. Figure 11 shows the  $xy$  component of the magnetoconductivity tensor  $\sigma_{xy}$  vs. magnetic field under dark, thermal equilibrium conditions, at four different temperatures. At lower temperatures (77 and 100 K), only heavy and light holes can be seen, as expected. However, at 135 K, the presence of a relatively small number of electrons

(minority carriers) can be observed and studied. At 160 K, the small number of intrinsic electrons thermally excited across the gap totally dominates electronic transport at low magnetic fields.

A Tektronix transient digitizer was used to capture the transient behavior of  $\sigma_{xy}$ , allowing us to show the effect of a  $\text{CO}_2$  laser pulse (full width at half maximum - 98 nsec) incident on the sample in Figure 12. The laser wavelength ( $9.25 \mu\text{m}$ ) was chosen such that two-photon excitation occurs at  $T = 50 \text{ K}$ , and the minority electrons generated can be observed and studied. Figure 12 shows the following four sets of transient digitizer data and theoretical curves: (1) In the dark, at a time before the laser pulse is incident on the sample; (2) At the peak of the laser pulse; (3) 325 nsec after the start of the laser pulse; and (4) 515 nsec after laser pulse onset. Note that the peak of the signal occurs approximately at the end of the laser pulse. Figure 12(c) shows how the variation can be curve fit to obtain information about the photoexcited electrons. Figure 13 shows a plot of the time dependence of the number of minority carriers (electrons). By way of comparison, we also plot the time variation of the photoconductive (pc) response, which is shown to be much slower. Details of the analysis are given in the above reference.

The behavior of the transient response is shown in Figure 14 for several temperatures between 10 and 160 K. Quite complex behavior is seen which is difficult to explain by itself. However, by using the magnetoconductivity tensor component analysis technique, we can show that the relatively fast decay at 120 and 160 K is due to minority carrier electrons. At lower temperatures, a two-stage decay is observed; the first (faster) decay arises from hole recombination involving shallow acceptor levels, and the second (longer) decay is due to hole recombination involving deep levels.

Finally, in Figure 15, the temperature dependence of the minority carrier (electron) lifetimes obtained from our analysis is shown. Again, for comparison purposes, we show the pc response as well. In those instances where two-stage decay occurs, we always plot the shorter decay. At temperatures greater than 160 K, the pc response lifetime is the same as that measured by analysis - the "true" minority carrier lifetime. Of particular interest is the use of this plot to determine the activation energy of the defect trap level which controls the electron lifetimes. Our data are consistent with a defect trap energy of 116 meV above the valence band - obviously the well documented mid-gap level. It is thus obvious that detailed information, not available through the study of only the pc response, can be obtained through the magnetoconductivity tensor component analysis method.

Work is now commencing on the analysis of samples of p-HgCdTe by the same method. Figure 16 shows the pc response of a sample ( $x = 0.307$ ) at various temperatures. Complex, two stage behavior can be seen, and at low temperatures, the hyperbolic nature of the transient response indicates that two-photon absorption is occurring.

### Summary

We have developed a novel method to characterize and measure the minority carrier lifetimes in semiconductors, and have successfully applied the method to P-InSb. The method offers the possibility of modeling decay mechanisms involving shallow deep, and mid-gap impurity and/or defect levels.

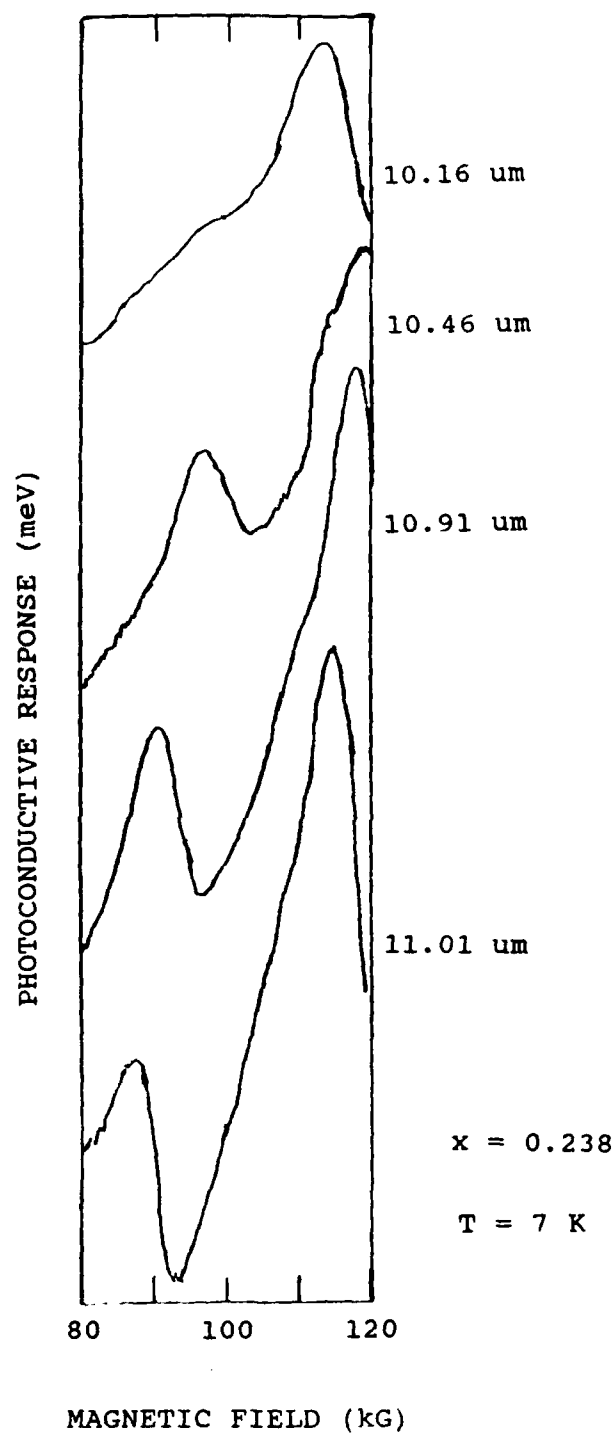


Figure 1. Wavelength dependence of the photoconductive response showing the two-photon absorption structure.

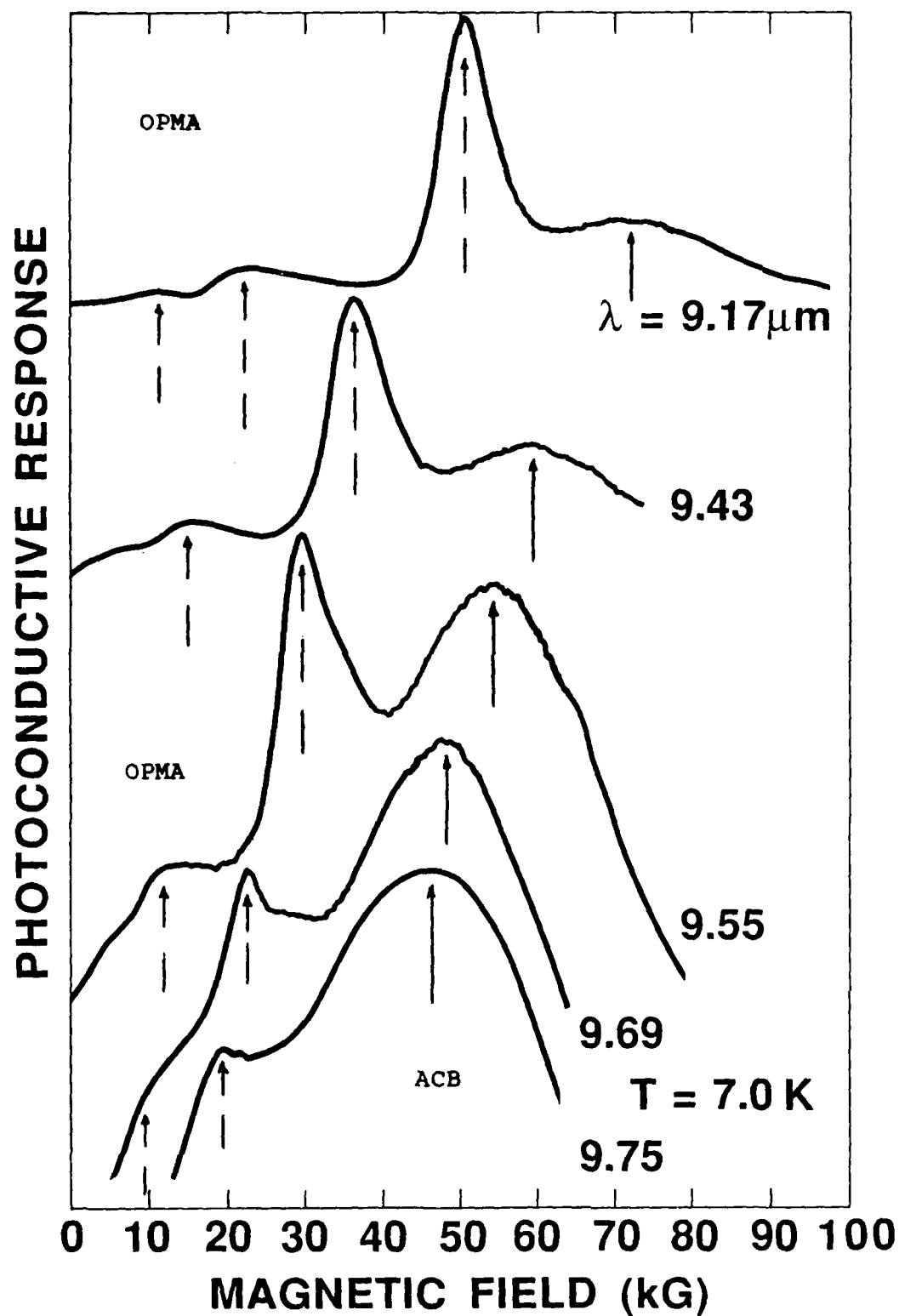


Figure 2. Wavelength dependence of the photoconductive response showing one-photon absorption (OPMA - dashed arrows), and acceptor to conduction band transitions (ACB - solid arrows).

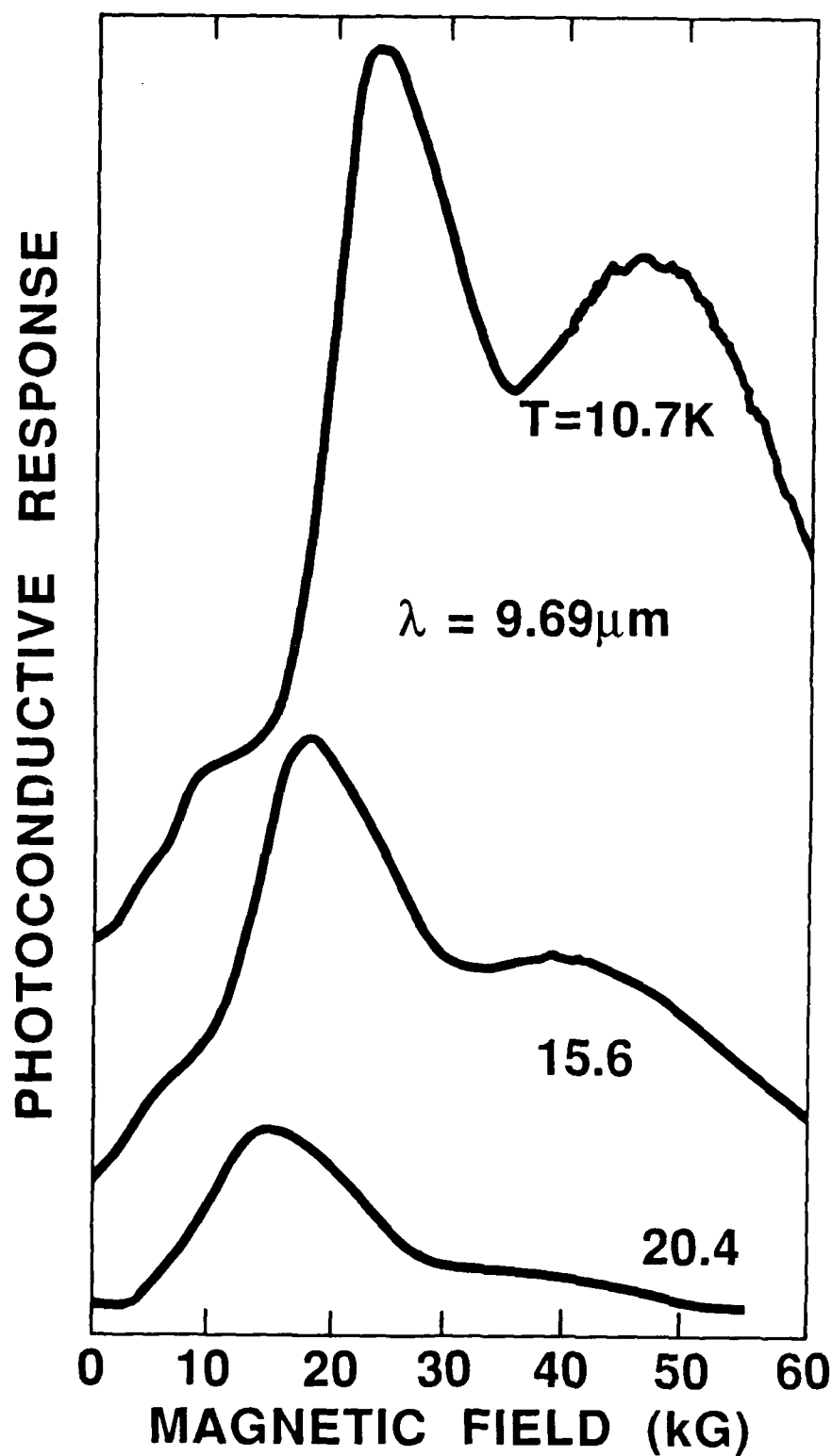


Figure 3. Temperature dependence of the one-photon absorption (OPMA) structure, and the acceptor to conduction band (ACB) absorption structure.

PHOTOCONDUCTIVE RESPONSE

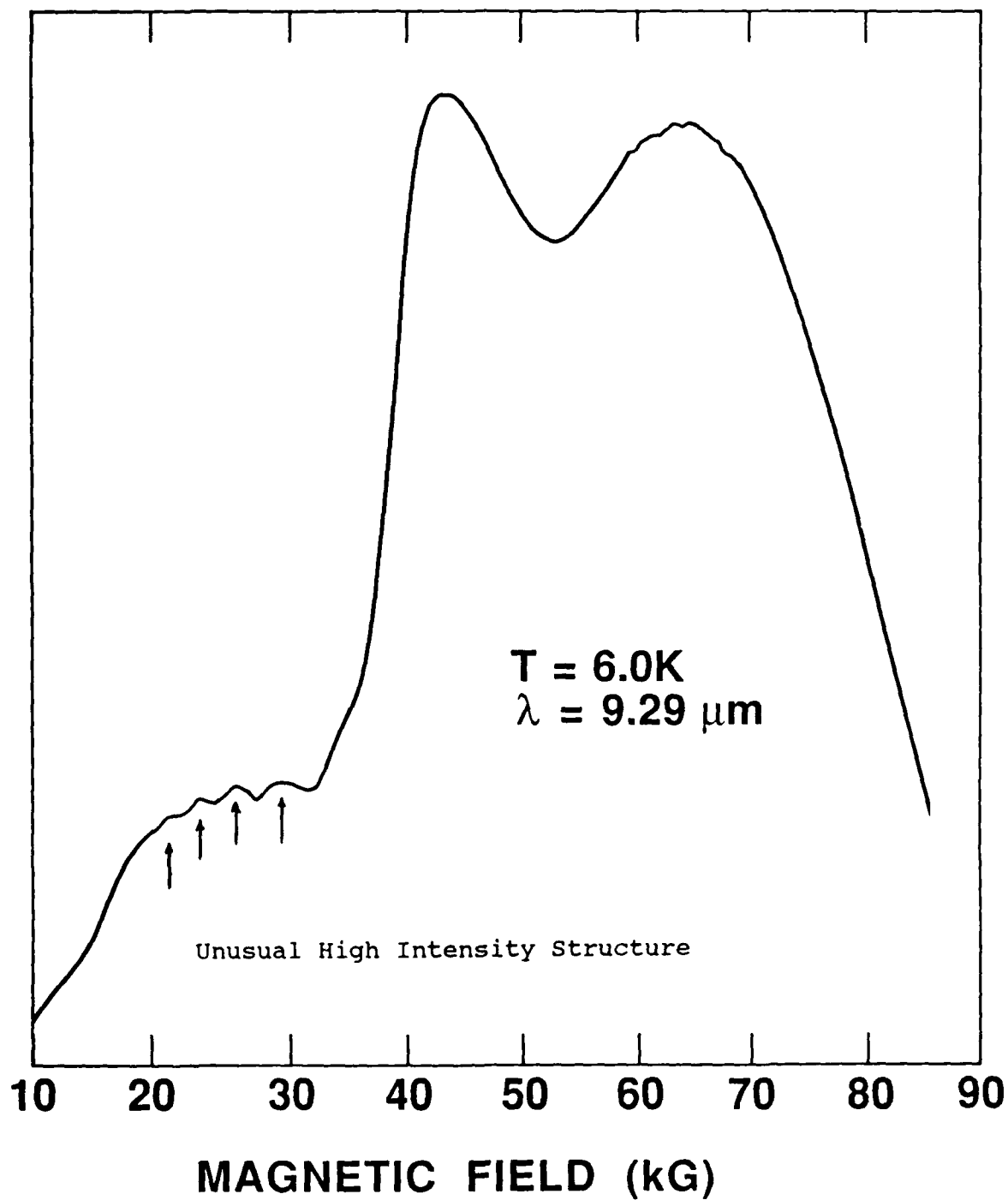


Figure 4. Complete magneto-absorption spectrum showing OPMA, ACB, and unusual high intensity structure

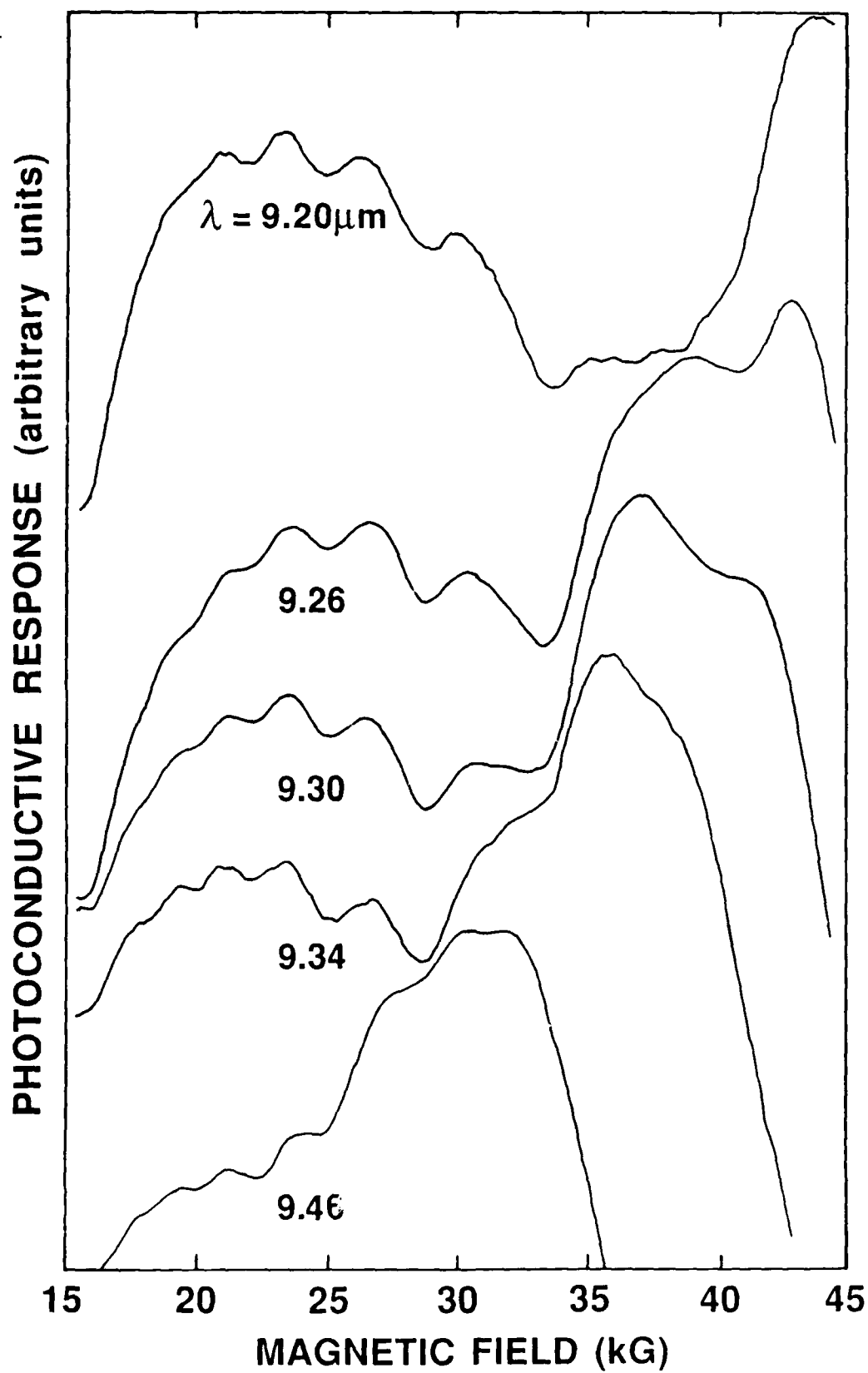


Figure 5. Unusual high intensity structure shown in expanded scale.

CAQE High Magnetic Field Lab  
Photon Energy vs. Magnetic Field

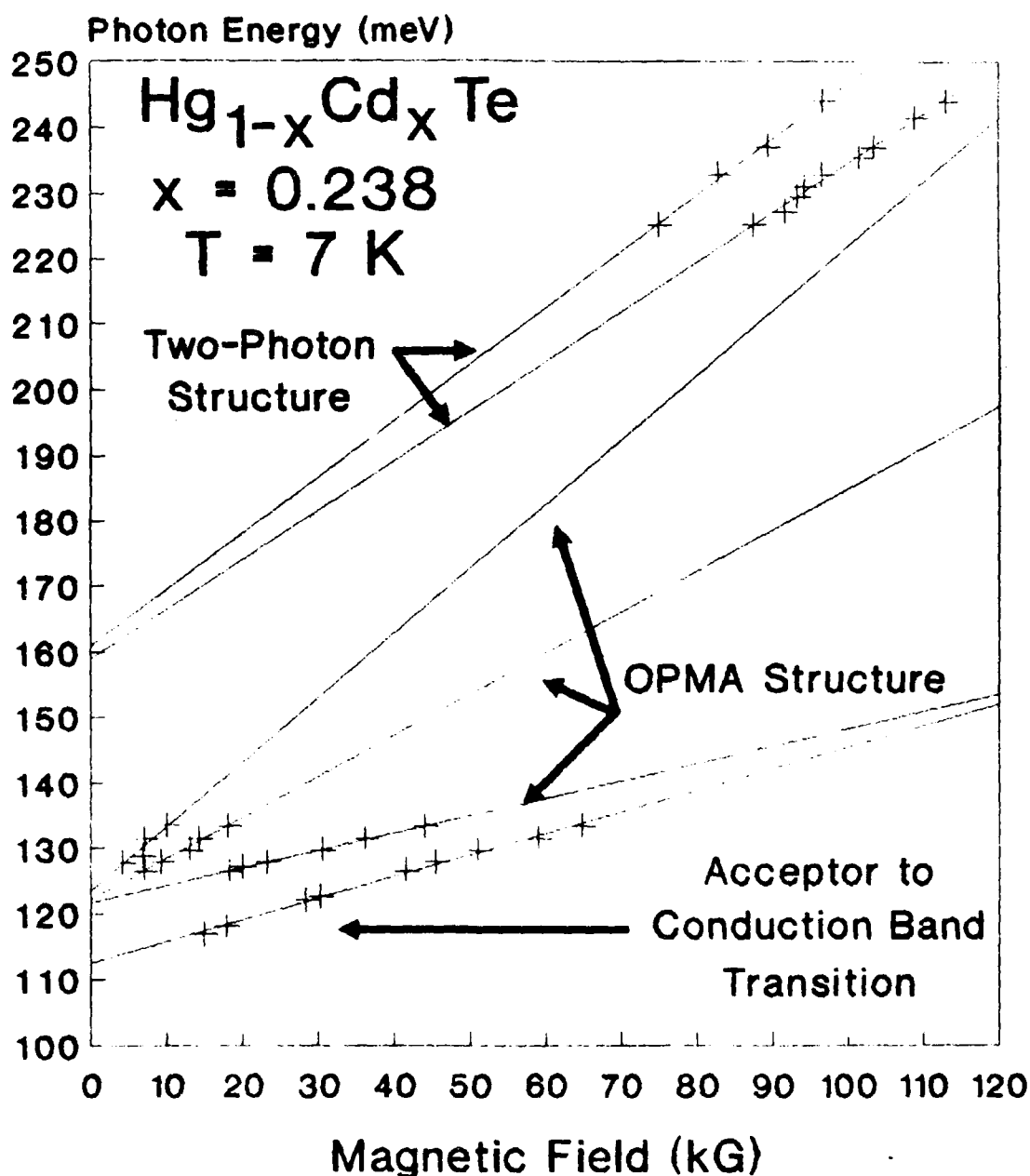
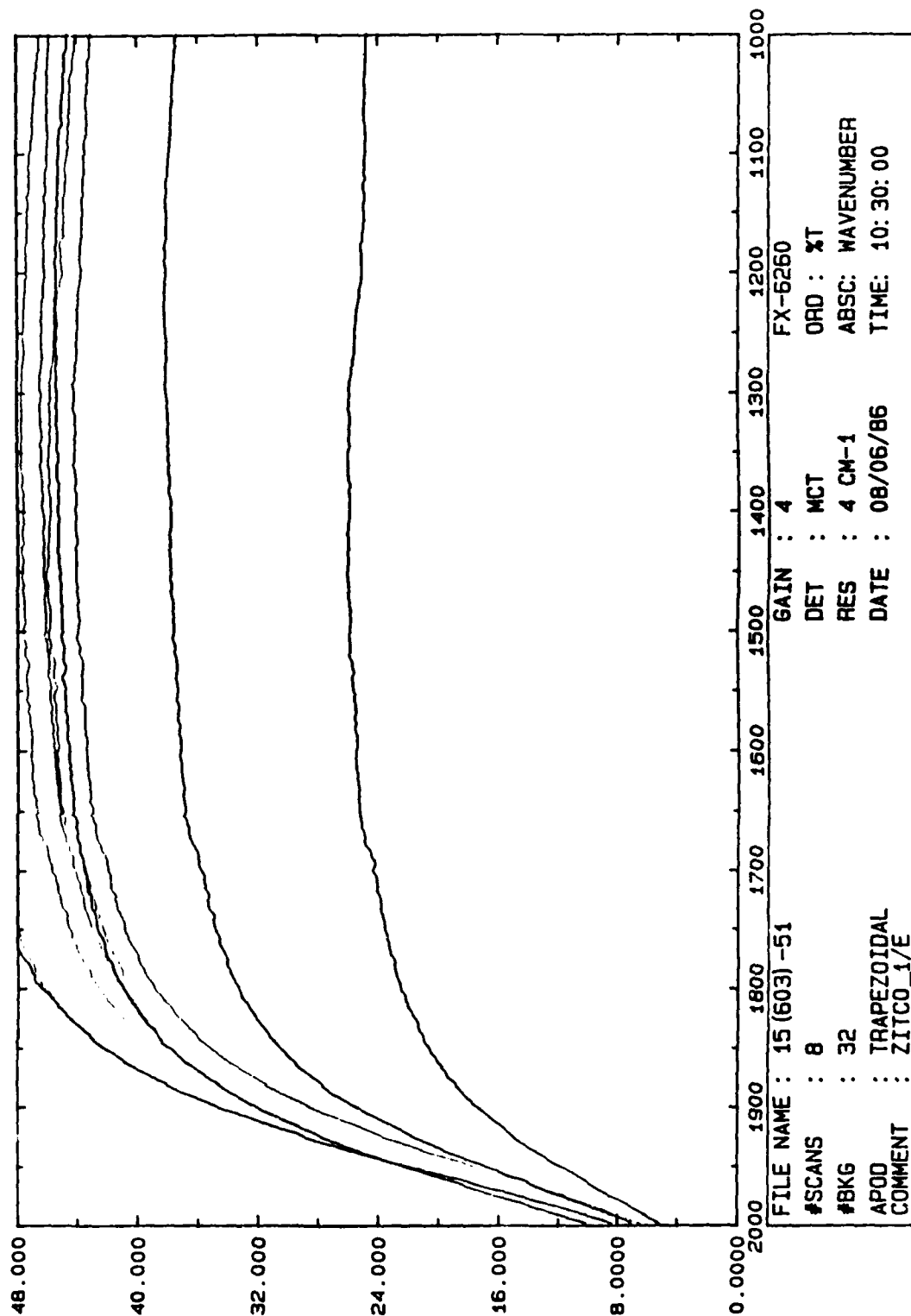


Figure 6. Photon absorption resonance positions vs. magnetic field.

POINT CUTON FREQUENCY 370°

U.L. :	2031.87
U.C. :	2024.15
U.R. :	2035.73
M.R. :	2033.16
C.L. :	2021.58
M.L. :	2030.58
U.C. :	2038.30
L.C. :	2029.30
L.R. :	2025.44

Figure 7. Cominco's transmission data for  $x = 0.26$  sample.



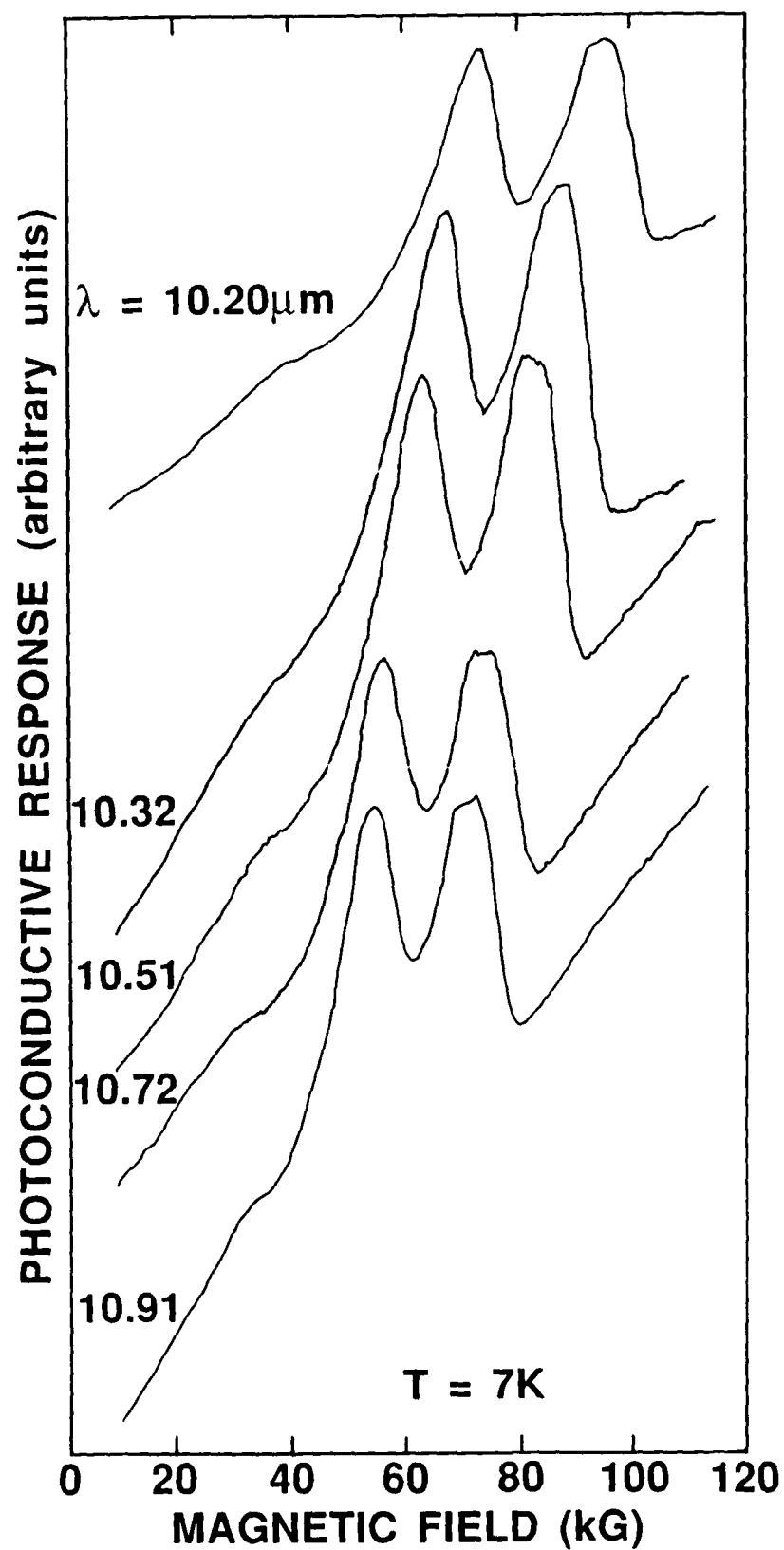
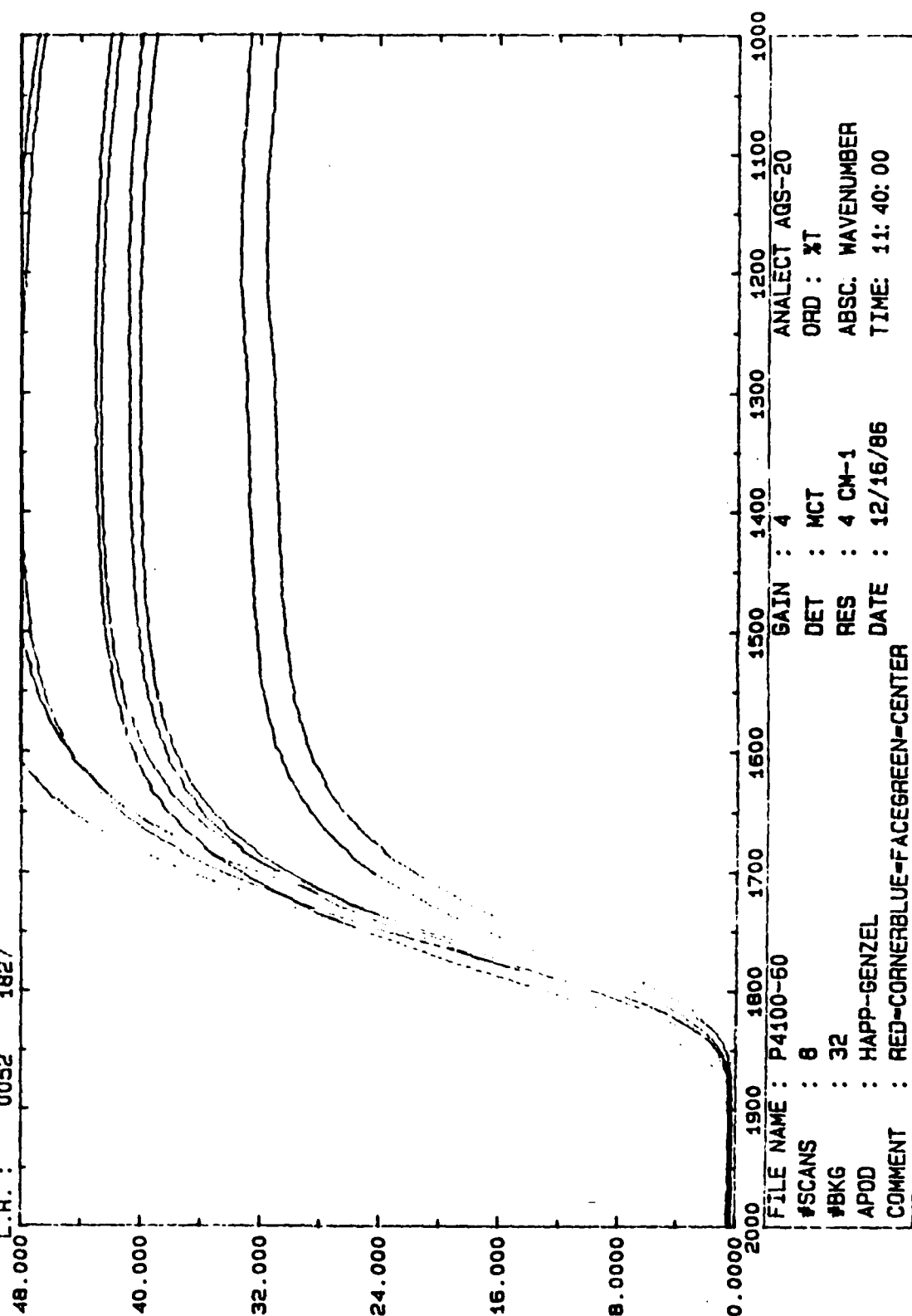


Figure 8. Photoconductive response vs. magnetic field for  $x = 0.26$  sample. Note the two-photon absorption peaks.

POINT MAX TRANS% 1/E\_ZITCO WN  
 U.L.: 0031 1827  
 U.C.: 0042 1833  
 U.R.: 0048 1818  
 M.R.: 0048 1836 MAX. = 1850  
 C.: 0043 1850  
 M.L.: 0040 1841 MIN. = 1818  
 L.L.: 0033 1832  
 L.C.: 0040 1845  
 L.R.: 0052 1827

TEMPERATURE 27.0 C

Figure 9. Cominco's transmission data for x = 0.27 sample.



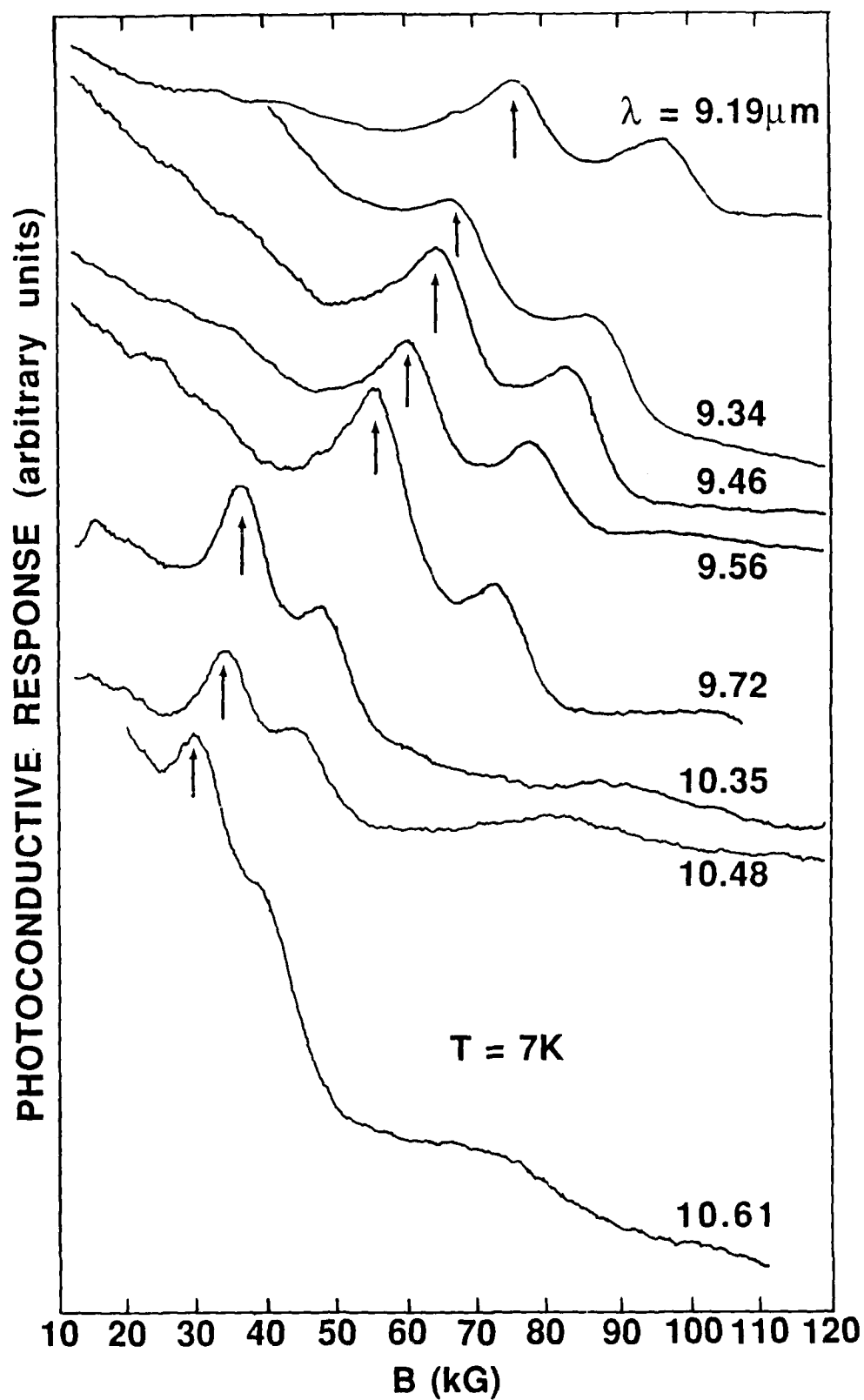
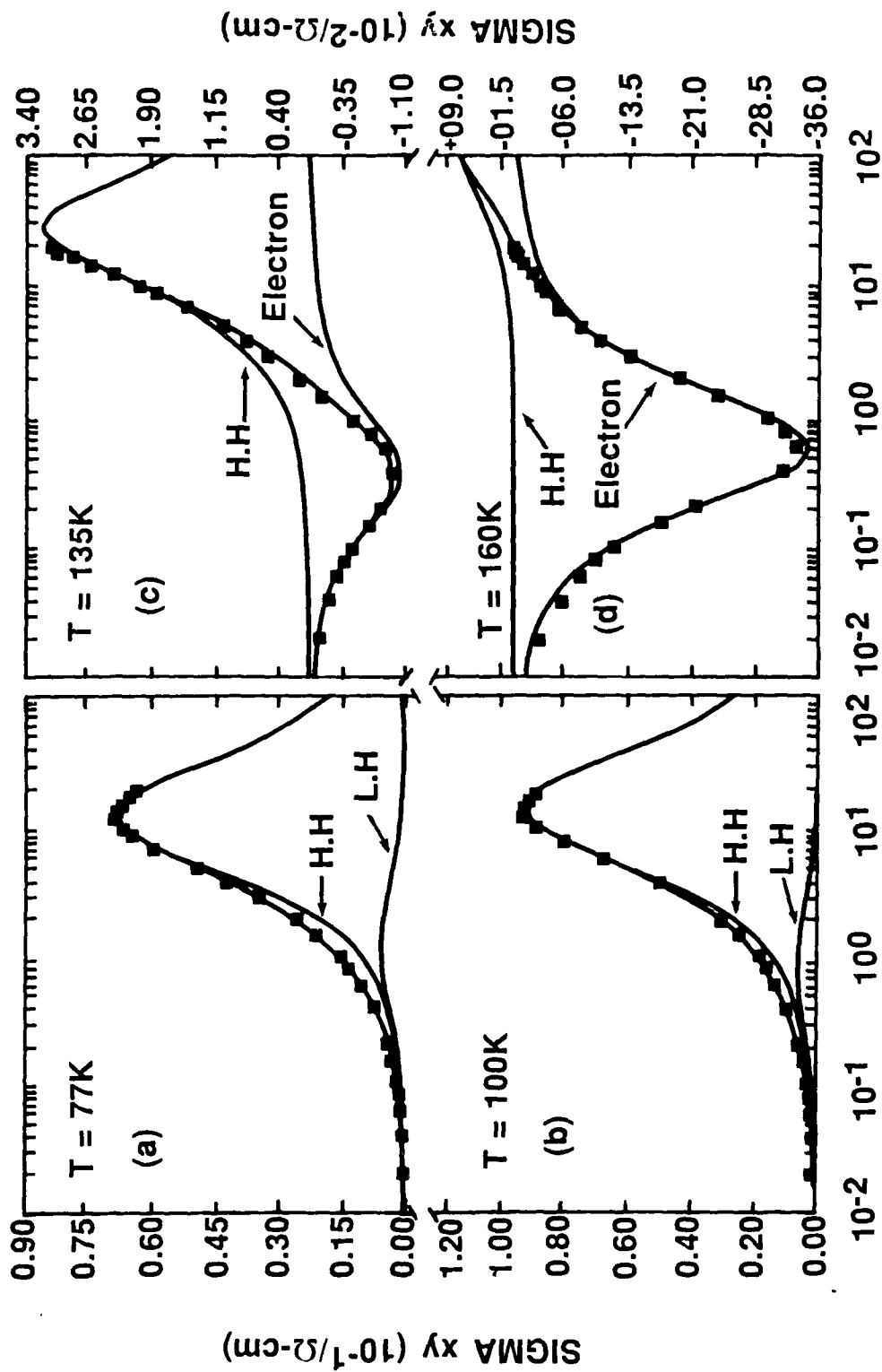


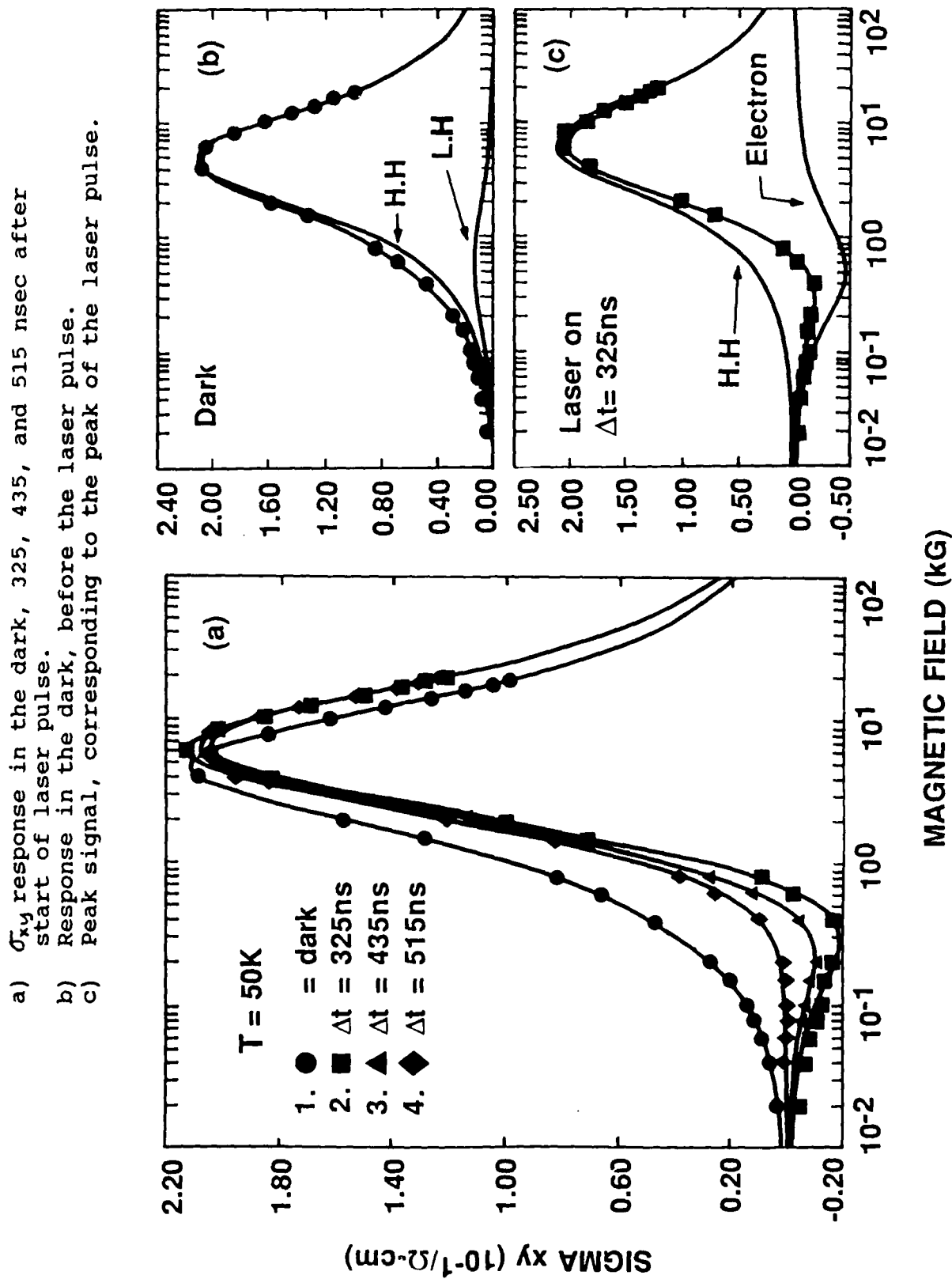
Figure 10. Photoconductive response vs. magnetic field for  $x = 0.27$  sample. Note the two-photon absorption peaks.



MAGNETIC FIELD (kG)

Figure 11.  $\sigma_{xy}$  vs. magnetic field for various temperatures.

Figure 12. Time resolved data:



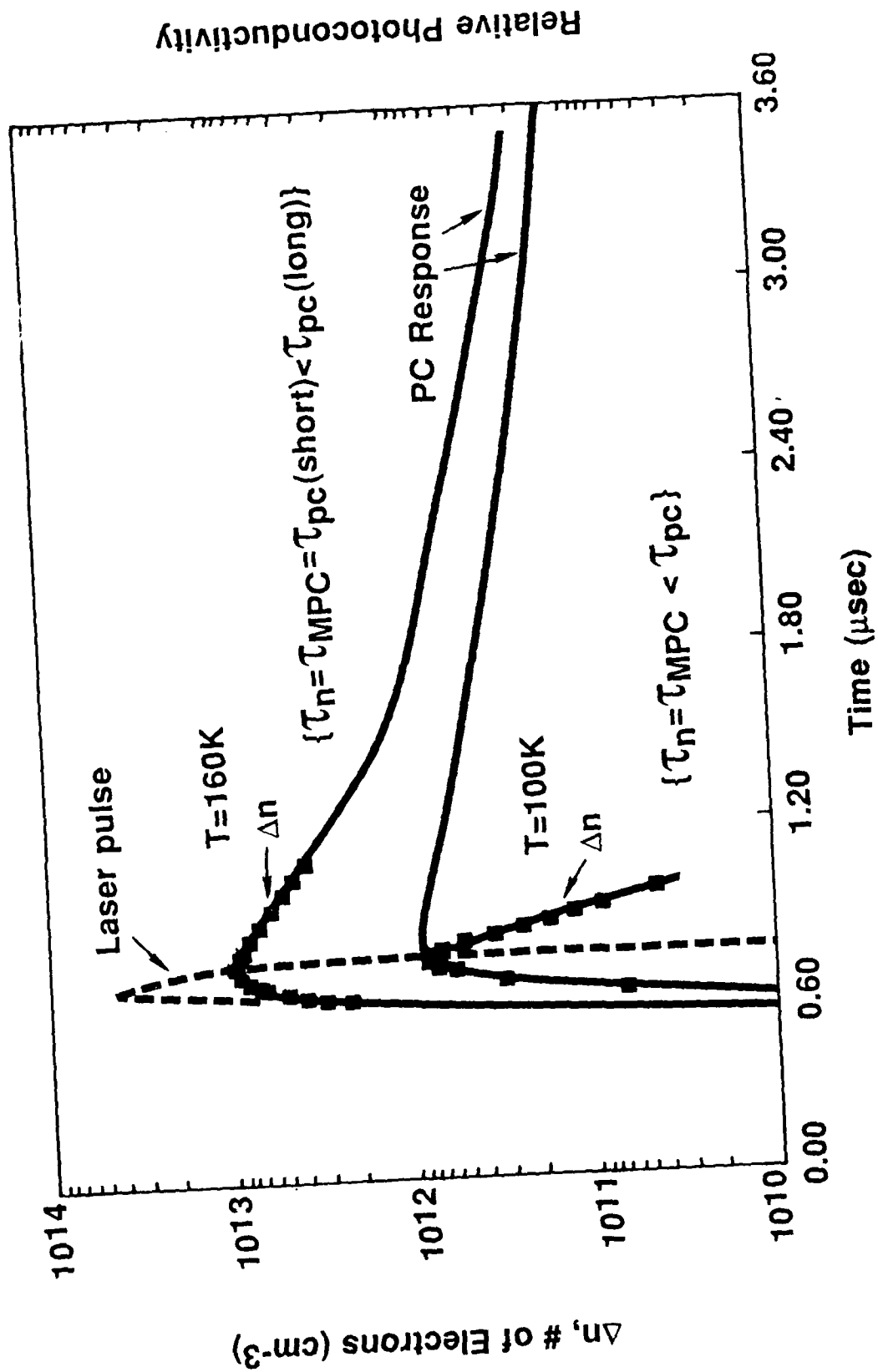


Figure 13. Comparison of the photoconductive and the magneto-photoconductive responses.

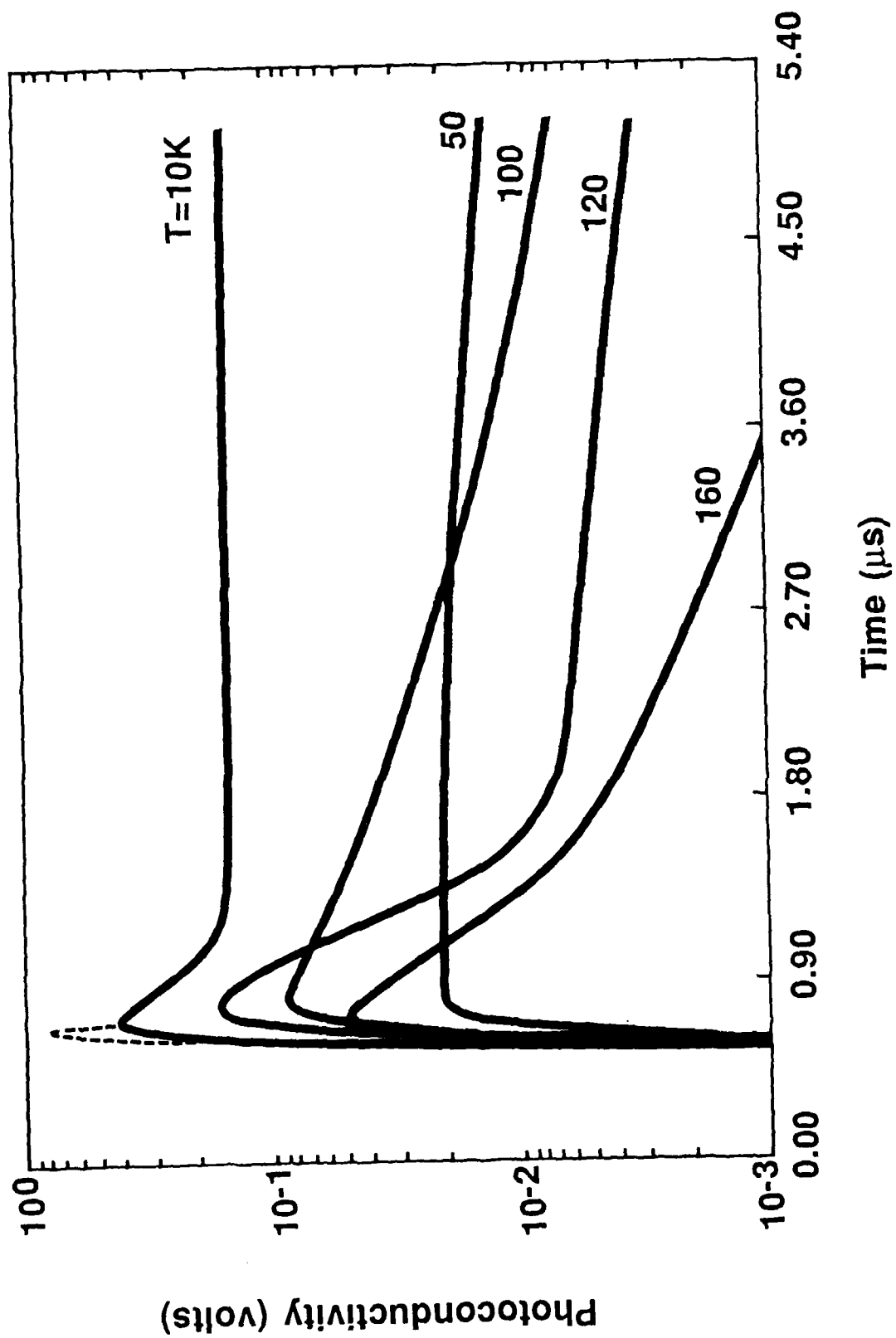


Figure 14. Transient photoconductive response.

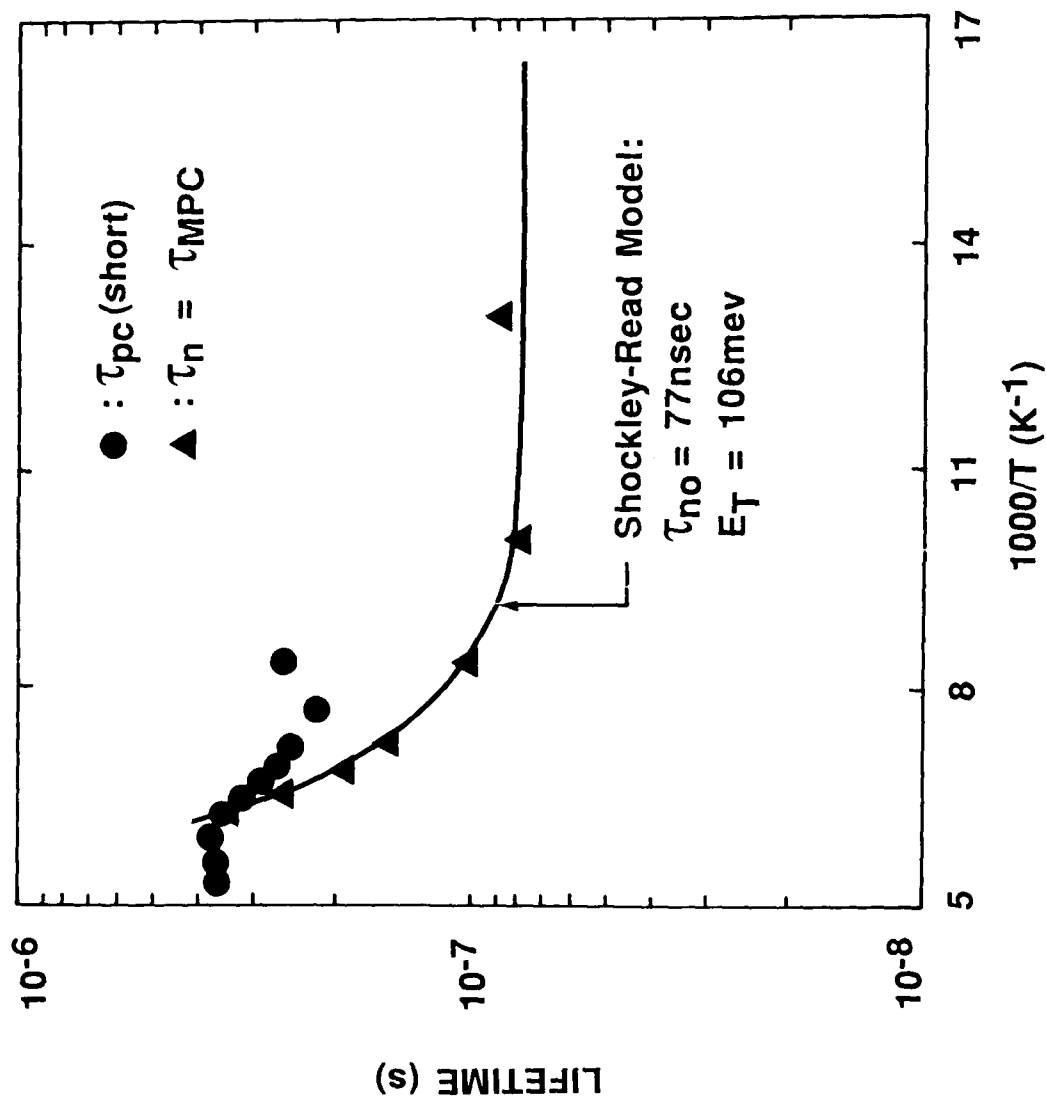


Figure 15. Lifetime (in nsec) vs. 1000/T. The triangles are minority (electron) lifetimes from  $\alpha_y$  analysis.

# PC Transient Response

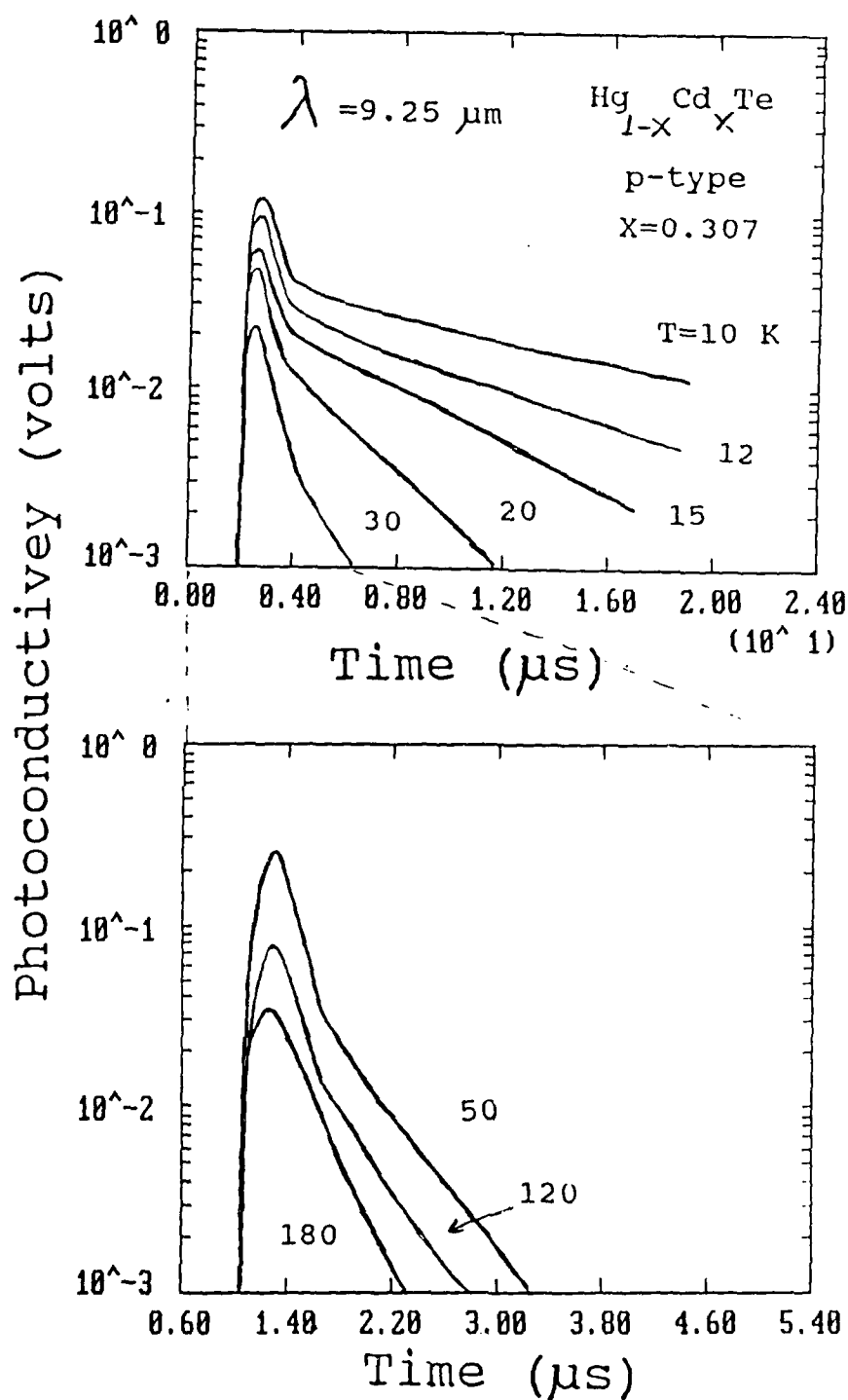


Figure 16. Transient photoconductive response at various temperatures.

# New method of characterizing majority and minority carriers in semiconductors

D. L. Leslie-Pelecky, D. G. Seiler, and M. R. Loloee

Center for Applied Quantum Electronics, Department of Physics, North Texas State University, Denton, Texas 76203

C. L. Littler

Central Research Laboratories, Texas Instruments, Inc., Dallas, Texas 75265

(Received 13 July 1987; accepted for publication 5 October 1987)

A novel characterization method using magnetoconductivity tensor components to determine the carrier concentration and mobility of majority and minority carriers is presented. Results are given for bulk  $n$ -HgCdTe (one carrier), liquid phase epitaxial  $n$ -HgCdTe (two carriers), and  $p$ -InSb (two or three carriers). Advantages of this method over the standard Hall coefficient analysis are discussed.

Advances in the improvement and application of new semiconducting materials (the use of HgCdTe in infrared detectors, for example) have necessitated an increased interest in the properties of minority carriers. Although Hall coefficient ( $R_H$ ) and magnetoresistance measurements have historically been used to characterize semiconductors by determining the carrier concentration ( $n$ ), mobility ( $\mu$ ), and relaxation time ( $\tau$ ) of the majority carriers, the form of the multicarrier Hall coefficient makes detailed information about minority carriers difficult to obtain. In this letter, we show that the complete magnetic field dependence of the magnetoconductivity provides more information than the traditional  $R_H$  measurement and analysis, allowing us to determine  $n$ ,  $\mu$ , and  $\tau$  for all carriers. Magnetoconductivity tensor components, which have the distinct advantage of being additive in the case of more than one carrier, have previously been used to characterize metals.<sup>1-3</sup> We demonstrate the power and ease of this method through application to bulk  $n$ -type  $\text{Hg}_{1-x}\text{Cd}_x\text{Te}$  (one carrier conduction),  $n$ -type liquid phase epitaxial (LPE) HgCdTe (two carriers), and  $p$ -type InSb (two-carrier conduction at low temperatures and three-carrier conduction at temperatures  $\approx 125$ –140 K).

The solution of the Boltzmann equation using a relaxation time approximation (RTA) has been detailed by Beer and others.<sup>4-6</sup> By finding the current density in terms of the electric field, the conductivity tensor may be identified. For a sample in the standard Hall configuration ( $\mathbf{H} = H\hat{z}$ ), the conductivity tensor components may be written:

$$\sigma_{xx} = \frac{\rho_{xx}}{\rho_{xx}^2 + R_H^2 H^2} \approx \sum_{i=1}^M \frac{n_i |e| H_i}{H_i^2 + H^2}, \quad (1a)$$

$$\sigma_{xy} = \frac{R_H H}{\rho_{xx}^2 + R_H^2 H^2} \approx \sum_{i=1}^M \frac{n_i e H}{H_i^2 + H^2}, \quad (1b)$$

where  $\rho_{xx}$  and  $R_H$  are the standard measured quantities of transverse magnetoresistance and Hall coefficient, respectively,  $M$  is the number of carrier types, the critical magnetic field  $H_i \approx 1/\mu_i = m^*/\tau_i e$ , in which  $\mu_i$  and  $\tau_i$  are average quantities.<sup>7</sup>  $n_i$  is the concentration of carriers of type  $i$  and  $e < 0$  for electrons. The applicability of the relaxation time approximation (RTA) to our mobility considerations might be questioned, since optical phonon scattering (inherently inelastic) is one of the dominant modes in compound semi-

conductors.<sup>8</sup> However, as shown by Pfeffer and Zawadzki<sup>9</sup> for InSb at room temperature, the variational mobility calculation for optic phonon scattering gives almost the same result as the RTA. As the temperature is lowered, the RTA becomes progressively less and less valid, but also the optic phonon contribution to the mobility becomes less important. For example, at 77 K and an electron concentration of  $10^{16} \text{ cm}^{-3}$ , the experimental mobility of electrons in  $n$ -InSb is  $10^5 \text{ cm}^2/\text{V s}$ , (Ref. 8) while the optic phonon contribution is  $1.5 \times 10^6 \text{ cm}^2/\text{V s}$ .<sup>9</sup> The elastic modes of scattering by ionized impurity and acoustic phonons can be treated by RTA. Thus, within the above approximations, the calculated individual relaxation times have physical meaning.

Note that  $\sigma_{xx}$  is positive for all carriers, while  $\sigma_{xy}$  will be negative for electron conduction and positive for hole conduction. Because of the differences in sign, we choose to fit  $\sigma_{xy}$  data, as differences in types of carriers become obvious upon plotting the experimental data. For  $\sigma_{xy}$ , the maximum value occurs when  $H = H_i$  and is proportional to  $n_i$  ( $\sigma_{xy} = n_i e / 2H_i$ ). Because of the simple algebraic form of Eq. (1b) and the ease with which partial derivatives are taken, any nonlinear least-squares fit is sufficient for fitting Eq. (1b) to the experimental  $\sigma_{xy}$  data as determined from the right-hand side of Eq. (1b).

Figure 1 shows  $\sigma_{xy}$  vs  $\ln H$  at 77 K for a bulk  $n$ -type  $\text{Hg}_{1-x}\text{Cd}_x\text{Te}$  sample, grown by the solid-state recrystallization method ( $x \approx 0.23$ ). The negative values of  $\sigma_{xy}$  indicate that conduction occurs by electrons. From the form of Eq. (1b), where  $M = 1$ , we see that the  $(x, y)$  coordinate describing the peak of the curve corresponds to the pair

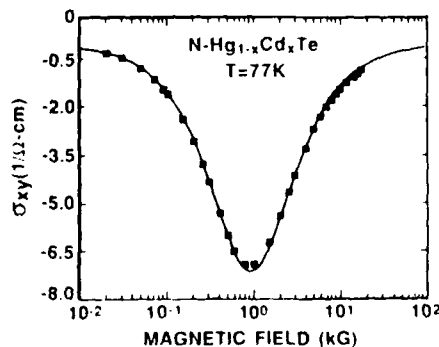


FIG. 1.  $\sigma_{xy}$  vs  $\ln H$  for  $n$ -type HgCdTe at 77 K.

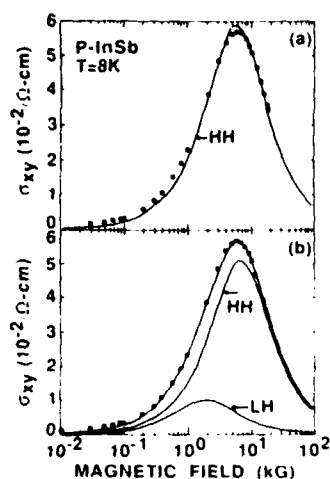


FIG. 2. (a) and (b) *p*-type InSb at 8 K: A simple, one-carrier Hall coefficient analysis finds  $7.04 \times 10^{13}$  carriers/cm<sup>3</sup> with mobilities of  $1.51 \times 10^4$  cm<sup>2</sup>/V s at  $B = 1$  kG and  $7.6 \times 10^{11}$  carriers/cm<sup>3</sup> with mobility of  $1.40 \times 10^4$  cm<sup>2</sup>/V s at  $B = 19$  kG. Note that there is negligible magnetic carrier freeze-out at these low fields (see Fig. 3 also).

$[H_i, \sigma_{xy}(\max)]$ . The coordinates of the peak therefore provide initial guesses for parameters in the curve fitting program. Using a standard nonlinear least-squares fit to Eq. (1b), we find  $n = 8.31 (\pm 0.11) \times 10^{14}$  cm<sup>-3</sup> and  $\mu = 1.08 (\pm 0.12) \times 10^5$  cm<sup>2</sup>/V s. Taking  $m^* = 0.01m_0$ ,  $\tau = 6.14 (\pm 0.68) \times 10^{-13}$  s. The Hall coefficient (at  $B = 1$  kG) yields  $n = 8.83 \times 10^{14}$  cm<sup>-3</sup>,  $\mu = 1.07 \times 10^5$  cm<sup>2</sup>/V s, and  $\tau = 6.08 \times 10^{-13}$  s in good agreement.

Figures 2(a) and 2(b) show  $\sigma_{xy}$  vs  $\ln H$  for a *p*-type InSb sample at 8 K. Figure 2(a) is an attempt to fit the data with a heavy-hole term only. Note that while the fit around the peak is satisfactory, the fit undercuts the data at low magnetic fields. In Fig. 2(b), both heavy- and light-hole carrier terms are included in order to accurately describe the data. By decomposing the fit into its constituent light- and heavy-hole terms, and identifying the peak coordinates,  $n$ ,  $\mu$ , and  $\tau$  may be determined for each type of carrier. Table I summarizes the numerical data found from both fits. In order to calculate  $\tau$ , the following effective mass values were used:  $m^*$ (light holes) =  $0.015m_0$  and  $m^*$ (heavy holes) =  $0.45m_0$ .<sup>10</sup> Because the terms in the magnetoconductivity are additive,  $\sigma_{xy}$  plots yield much more information in the complex situations often encountered in the laboratory in terms of concentrations and types of carriers than

TABLE I. Summary of numerical data found by one-carrier and two-carrier fits of  $\sigma_{xy}$  data for *p*-type InSb at 8 K to Eq. (1b)

	Fig. 2(a) One-carrier fit	Fig. 2(b) Two-carrier fit
Light holes		
$p$ (cm <sup>-3</sup> )		$2.82 (\pm 0.06) \times 10^{12}$
$\mu$ (cm <sup>2</sup> /V s)		$5.08 (\pm 0.46) \times 10^4$
$\tau$ (s)		$4.32 (\pm 0.39) \times 10^{-13}$
Heavy holes		
$p$ (cm <sup>-3</sup> )	$4.23 (\pm 0.09) \times 10^{13}$	$4.28 (\pm 0.05) \times 10^{13}$
$\mu$ (cm <sup>2</sup> /V s)	$1.81 (\pm 0.36) \times 10^4$	$1.48 (\pm 0.01) \times 10^4$
$\tau$ (s)	$4.62 (\pm 0.92) \times 10^{-12}$	$3.79 (\pm 0.03) \times 10^{-12}$
Standard deviation	$8.20 \times 10^{-5}$	$4.57 \times 10^{-6}$

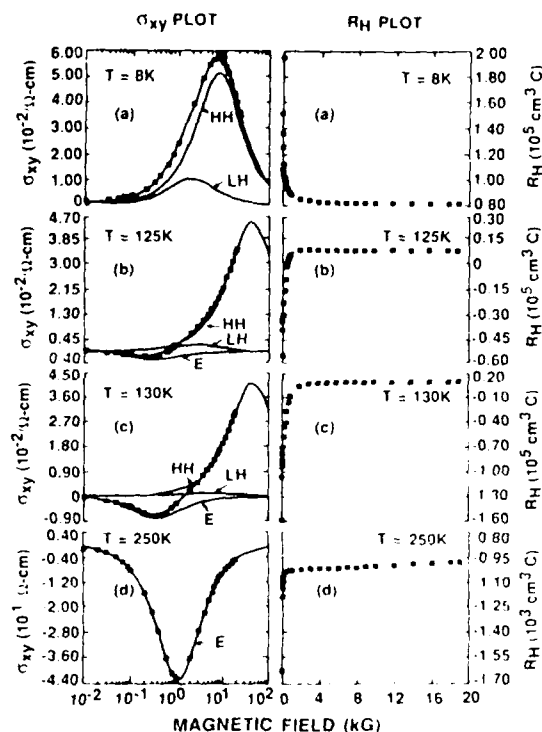


FIG. 3. Comparison of the Hall coefficient and  $\sigma_{xy}$  plots for *p*-type InSb for various temperatures (a) 8 K, (b) 125 K, (c) 130 K, (d) 250 K. Note the sensitivity of the  $\sigma_{xy}$  plot to small changes in temperature.

do standard Hall coefficient plots. An example of this is seen in Fig. 3 where the  $\sigma_{xy}$  plots are compared with their corresponding Hall coefficient plots for a *p*-InSb sample for  $T = 8$ –250 K. The  $\sigma_{xy}$  curve at 8 K indicates that there are both light holes and heavy holes present, as discussed previously. In addition to the light and heavy holes already present, electronic contributions to conduction are apparent as  $\sigma_{xy}$  takes on negative values at low fields at 125 K. Note that the small concentrations of electrons present (on the order of  $10^{11}$  cm<sup>-3</sup>) relative to the concentration of heavy holes present (on the order of  $10^{14}$ ) are much more apparent in the  $\sigma_{xy}$  curve than in the corresponding Hall plot. At 130 K, a temperature change of only 5 K, the  $\sigma_{xy}$  curve has changed noticeably in both the height and critical magnetic field of the electron peak. Because of the large concentration of heavy holes and relatively small change in concentration of

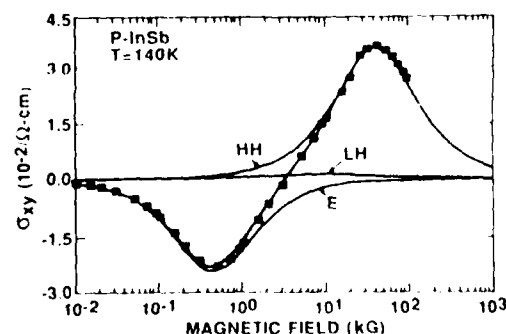


FIG. 4. Three-carrier fit of  $\sigma_{xy}$  data for *p*-type InSb at 125 K. Data taken at Francis Bitter National Magnet Lab.

TABLE II. Numerical data obtained by a three-carrier fit of  $\sigma_{xy}$  data for  $p$ -type InSb at 140 K.

	Electrons	Heavy holes	Light holes
$n(\text{cm}^{-3})$	$1.44(\pm 0.02) \times 10^{12}$	$1.75(\pm 0.02) \times 10^{14}$	$1.50(\pm 1.49) \times 10^{12}$
$\mu(\text{cm}^2/\text{V s})$	$2.18(\pm 0.28) \times 10^5$	$2.52(\pm 0.05) \times 10^3$	$1.14(\pm 0.69) \times 10^4$
$\tau(\text{s})$	$5.57(\pm 0.72) \times 10^{-11}$	$6.44(\pm 0.13) \times 10^{-13}$	$2.91(\pm 1.76) \times 10^{-10}$

electrons, the Hall coefficient curve is not significantly changed. At 250 K, the conduction is mainly due to electrons as shown by the one carrier band fit. Overall, the  $\sigma_{xy}$  components, which can be easily decomposed, are much more illustrative in their description of transport properties than corresponding Hall coefficient plots.

Because of the low mobility of the predominant heavy holes, peaks in the  $\sigma_{xy}$  plots are not always possible to observe with low magnetic fields, thus making quantitative fitting difficult. Figure 4 shows the results of high field measurements made at the Francis Bitter National Magnet Laboratory on a  $p$ -type InSb sample at 140 K that quantitatively demonstrates the sensitivity of our technique. In this sample, we are able to quantitatively characterize light holes, heavy holes, and electrons. Numerical values are summarized in Table II. In calculating  $\tau$ , we have used  $m^*$  (light holes) =  $0.015m_0$ ,  $m^*$  (heavy holes) =  $0.45m_0$ , and  $m^*$  (electrons) =  $0.01m_0$ .<sup>10</sup> We find that the value obtained through the fit for the concentration and mobility of light holes is very reasonable compared to the number and mobility of the heavy holes present.

Figures 5(a) and 5(b) show the application of this

method to an epitaxially grown  $n$ -type LPE  $\text{Hg}_{1-x}\text{Cd}_x\text{Te}$  sample ( $x \approx 0.23$ ) at 15 K. This sample exhibited anomalous transport properties, i.e., a low mobility at low temperatures and peaks in both the Hall coefficient and mobility versus temperature data. Figure 5(a) shows an attempt to describe the  $\sigma_{xy}$  data using one carrier (electron), as would be expected for  $n$ -type conduction. It is seen that the conduction mechanisms in this sample are more complicated, as evidenced by the inability of the one-carrier model to adequately describe the  $\sigma_{xy}$  data. Subsequent attempts using combined electron and hole conduction to describe the data were equally unsuccessful. Figure 5(b) shows, however, that the data can be satisfactorily explained by using two electrons of vastly different mobility and concentration. These values are given in the caption of Fig. 5. We note that two-electron conduction has been previously reported by Finkman and Nemirovsky in bulk  $n$ -type  $\text{HgCdTe}$ .<sup>11</sup> In addition, a previous study<sup>12</sup> on LPE  $\text{HgCdTe}$  invoked a model of  $p$ -type inclusions in an  $n$ -type matrix to describe the anomalous carrier transport properties. However, our  $\sigma_{xy}$  data show no evidence of holes contributing to conduction in these anomalous samples.

Because of its simplicity and sensitivity to minority carriers, we predict that magnetoconductivity tensor analysis will join Hall coefficient and magnetoresistance analysis as a standard characterization tool in the semiconductor industry, applicable not only to bulk materials, but also to thin films and the new generations of artificially structure materials.

We acknowledge the partial support of this work by Texas Instruments and a Faculty Research Grant from North Texas State University. We thank Dr. D. Weinrauch for providing the LPE samples and Professor Wlodek Zawadzki for his helpful comments.

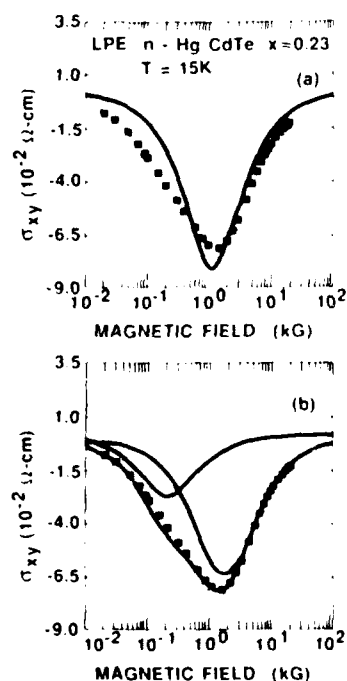


FIG. 5. (a) One-carrier fit. We find  $1.16(\pm 0.08) \times 10^{11} \text{ cm}^{-3}$  electrons with a mobility of  $8.90(\pm 0.58) \times 10^4 \text{ cm}^2/\text{V s}$ . (b) Two-electron fit. We find  $n_1 = 1.35(\pm 0.19) \times 10^{11} \text{ cm}^{-3}$ ,  $\mu_1 = 5.98(\pm 0.14) \times 10^4 \text{ cm}^2/\text{V s}$  and  $n_2 = 8.08(\pm 0.69) \times 10^{11} \text{ cm}^{-3}$ ,  $\mu_2 = 4.43(\pm 0.23) \times 10^4 \text{ cm}^2/\text{V s}$ . The Hall coefficient finds  $5.24 \times 10^{11} \text{ carriers cm}^{-3}$  with mobilities of  $4.5 \times 10^4 \text{ cm}^2/\text{V s}$  at  $B = 1 \text{ kG}$  and  $1.71 \times 10^{12} \text{ carriers cm}^{-3}$  with mobilities of  $1.4 \times 10^5 \text{ cm}^2/\text{V s}$  at  $B = 10 \text{ kG}$ .

<sup>1</sup>G. G. Gremier, J. M. Reynolds, and J. R. Sybert, *Phys. Rev.* **132**, 58 (1963).

<sup>2</sup>J. R. Sybert, H. J. Mackey, and K. L. Hathecox, *Phys. Rev.* **166**, 710 (1968).

<sup>3</sup>J. W. McClure, *Phys. Rev.* **112**, 715 (1958).

<sup>4</sup>A. C. Beer, *Galliummagnetic Effects in Semiconductors* (Academic, New York, 1963).

<sup>5</sup>A. H. Wilson, *The Theory of Metals*, 2nd ed. (Cambridge University, Cambridge, 1953).

<sup>6</sup>B. R. Nag, *Electron Transport in Compound Semiconductors* (Springer, New York, 1980).

<sup>7</sup>Z. Dziuba and R. Kowalczyk, *Phys. Status Solidi B* **119**, K11 (1983).

<sup>8</sup>W. Zawadzki, in *Handbook on Semiconductors*, edited by W. Paul (North-Holland, New York, 1982), Vol. 1, p. 713.

<sup>9</sup>P. Pfeffer and W. Zawadzki, *Phys. Status Solidi B* **88**, 247 (1978).

<sup>10</sup>C. L. Littler, D. G. Seiler, R. Kaplan, and R. J. Wagner, *Phys. Rev. B* **27**, 7473 (1983).

<sup>11</sup>E. Finkman and Y. Nemirovsky, *J. Appl. Phys.* **53**, 1052 (1982).

<sup>12</sup>M. C. Chen, S. G. Parker, and D. F. Weinrauch, *J. Appl. Phys.* **58**, 3150 (1985).

END  
DATE  
FILMED  
DTIC

11-88